IEEE Access
Multidisciplinary ⋮ Rapid Review ⋮ Open Access Journal

Received December 7, 2020, accepted December 18, 2020, date of publication December 22, 2020,
date of current version January 4, 2021.

Digital Object Identifier 10.1109/ACCESS.2020.3046626

Cooperative Control Strategy of Virtual Synchronous Generator Based on Optimal Damping Ratio

SHENGWEI QU AND ZHIJIE WANG
College of Electrical Engineering, Shanghai Dianji University, Shanghai 201306, China
Corresponding author: Zhijie Wang (wangzj@sdju.edu.cn)

This work was supported in part by the Shanghai Natural Science Foundation 15ZR1417300.

ABSTRACT Wind power, photovoltaics and other new energy sources are connected to the grid on a large scale. The power electronic interface cannot provide inertia and damping support for the microgrid. The virtual synchronous generator technology is introduced into the inverter control system. Unlike the synchronous generator, its parameters are flexible and adjustable, which can enhance the robustness of the microgrid. This paper firstly analyzes the influence of the moment of inertia and damping on the system, it is based on the equivalent relationship between the three-phase inverter and the synchronous machine, combined with the VSG rotor motion equation, and conducts stability analysis based on the small signal model and root locus. Based on the existing control strategy, a virtual synchronous generator cooperative control strategy based on the optimal damping ratio is proposed. Finally, the VSG collaborative control model is built in MATLAB/Simlink, the experimental results show that the proposed control strategy effectively improves the transient performance of the VSG, the system active power overshoot is reduced from 5% to 0, and the frequency deviation peak is lowered from 0.174 Hz to 0.115 Hz, which confirms the effectiveness of the proposed control strategy.

INDEX TERMS Microgrid, virtual synchronous generator, inertia, damping, cooperative control.

I. INTRODUCTION

The disadvantages continue to emerge, as for the traditional power generation relying on coal, oil and other fossil energy, such as environmental degradation and resource depletion. New energy power generation represented by photovoltaic and wind power is booming, and its proportion in the power grid has also increased, which also brings some new challenges [1]–[3]. Different from the traditional power system, new energy distributed generation is mostly operated in the form of micro-grid, which is connected to the large grid by inverter for unified management or consumed by the users of the distribution network nearby. However, inverter devices composed of power electronic devices cannot provide inertia and damping for the system to support grid stability. Meanwhile, the uncertainties of wind power and photovoltaic power generation make new energy power generation face many problems.

The associate editor coordinating the review of this manuscript and approving it for publication was Arup Kumar Goswami.

The Virtual synchronous generator (VSG) technology uses the characteristics of synchronous generators to improve the control system of new energy power generation equipment, so that grid-connected inverters have external characteristics of synchronous generators. At the same time, the VSG technology draws on traditional power system control strategies, make microgrid has the support ability of frequency and voltage regulation, and then actively participates in the operation and management of the grid [4], [5]. Unlike traditional synchronous generators, the virtual moment of inertia and damping coefficient (the J and the D for short) of the VSG can be changed according to the operating state of the system, enhancing the flexibility of microgrid operation [6]–[9]. A large number of scholars have carried out a lot of research on the VSG technology models, active/frequency control, and reactive voltage/control, etc., effectively promoting the application of virtual synchronous generator technology in microgrid [9]–[12]. Reference [2] shows the classification of virtual synchronous generator technology based on existing application scenarios, sorts out its typical applications,

and introduces parameter design and stability analysis at the same time, as well as the problems existing in the current virtual synchronization technology application to sum up, and summarizes the existing problems in the application of virtual synchronous technology at present. Reference [13], based on the analysis of the output characteristics of the J on VSG, proposes an improved adaptive control strategy for the J, which effectively curbs the excessive frequency change, but ignores the impact of the D on the system. Reference [14] establishes a VSG small signal model, analyzes the stability of the system when the D coefficient changes, and establishes an adaptive damping VSG control strategy to suppress the frequency overshoot oscillation, and the value of the J is not analyzed. References [15], [16] based on the synchronous motor swing equation, considering the J and the D, researching the VSG frequency and power fluctuations, using Lyapunov for stability analysis, and proposing a bang-bang control strategy to ensure system response time and comparison small overshoot. Reference [17] compares the operational characteristics between SG and VSG, such as Q-δ, P-f. Reference [18] proposed a voltage-controlled VSG technique to simulate the rotor inertia and system frequency modulation characteristics of SG in frequency control, to improve the frequency stability of the system.The power controller and voltage frequency controller make VSG perform functions of power control and frequency modulation [19], [20]. Reference [21] analyzes the influence of various parameters on system output characteristics, and proposes an adaptive control strategy for the J and the D, which effectively shortens the transient process of the system. Reference [22] introduces the importance of the VSG in modern power grids, and it provides a comprehensive review on the control and coordination of VSG toward grid stabilization in terms of frequency, voltage and oscillation damping during inertia response. Finally, perspective on the technical challenges and potential future research related to VSG is also discussed. Reference [23] summarizes the recent development in VSG control operation and discusses the current progress in distributed power generation and role of VSG. At the same time, it discusses in detail the difficulties of VSG and future research directions. The inverter adopting the VSG control strategy has the external characteristics and the J and the D characteristics of the synchronous generator. The above references consider the flexibility of the inverter control system, and perform parameter tuning or adaptive control on the J or the D, but the relationship between the two parameters has not been effectively analyzed.

The contribution of this paper is to combine the power characteristics of synchronous generators with the active loop transfer function of small signal analysis, the paper analyze the relationship between the J and D. Hence, the paper combines the existing control strategy and proposes a virtual synchronous generator cooperative control strategy based on the optimal damping ratio. When the system is disturbed, the system can respond quickly and adjust parameters automatically, thus effectively improving the dynamic performance of the system. Finally, the VSG cooperative control model is built in MATLAB/Simlink for experimental simulation. By comparing with constant parameter control and variable parameter control (bang-bang control strategy) [15], [16], proves the effectiveness and superiority of the proposed control strategy.

II. THE VSG MATHEMATICAL MODEL AND RATIONALE

As an integral part of distributed power sources, energy storage devices, system loads and electric energy conversion devices, microgrid can realize functions such as self-control protection and management [1]. Fig. 1 shows a typical microgrid structure. With the development of distributed energy and the disadvantages brought by the development of traditional energy, the microgrid gradually becomes an effective supplement to the large power grid due to its flexibility and environmental friendliness. The control system of the microgrid is based on characteristics such as output power, grid-connected voltage, output current, and system frequency. The main control strategies are: PQ control, V/ F control, Droop control. It is necessary to select an appropriate control strategy according to the operating conditions of stable power grid. The VSG technology uses characteristics such as inertia characteristics, damping characteristics, active frequency regulation, and reactive voltage regulation during operation of synchronous generator sets [2], [3], [8], which provides support for the stable operation of the system when the microgrid is isolated or connected to the grid, the VSG technology provides a better solution for the development of new energy and the application of microgrid.

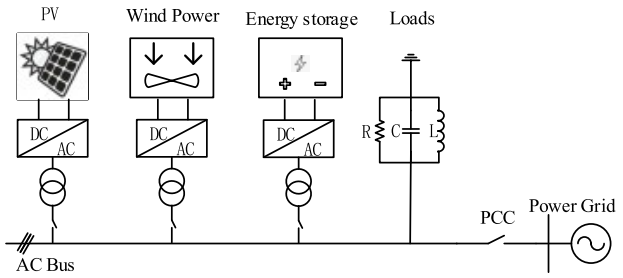

FIGURE 1. Microgrid structure diagram.

A. THE VSG MATHEMATICAL MODEL

Fig.2 is an equivalent diagram of the three-phase inverter and the synchronous generator. The new energy equipment such as wind, solar, and storage is equivalent to the prime mover, while the DC/AC three-phase inverter adopts the virtual generator control strategy, and is equivalent to synchronous generator, which can be analyzed by analogy with the prime mover driving synchronous generator model in the traditional power system. In the main circuit topology of the inverter, the U_{dc} is the DC input voltage, the e_{abc} is the VSG virtual electromotive force, the i_{abc} is the VSG output current, the L_f , R_f is the filter inductor, resistance, the u_{abc} is the common connection point voltage, the u_{gabc} is the grid voltage. In the synchronous generator model, the E is the

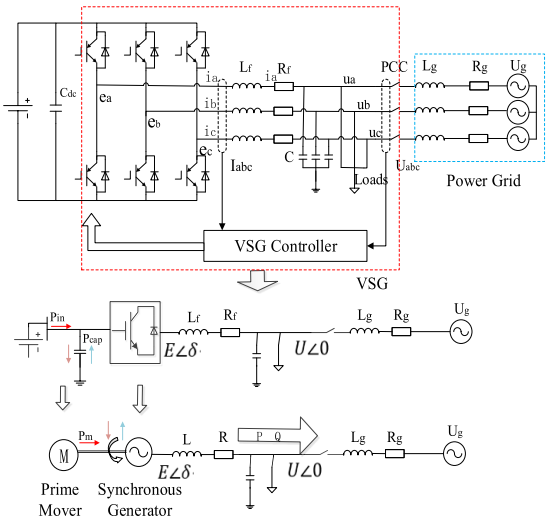

FIGURE 2. Equivalent diagram of three-phase inverter and synchronous generator.

electromotive force of the synchronous generator, the δ is the power angle of the synchronous generator, and U is the terminal voltage of the synchronous generator. the P, Q are the output active power and reactive power. It can be seen from the equivalent diagram that the midpoint voltage e_{abc} of the three-phase inverter bridge arm is used to simulate the electromotive force in the synchronous generator, and the equivalent inductance and resistance (L_f, R_f) at the side of the inverter can be equivalent to the stator end reactance of the synchronous generator, and the u_{abc} can be equivalent to the stator end voltage of the synchronous generator.

The key content of the VSG technology is to introduce the electromagnetic transient equation and rotor motion equation of the synchronous generator into the three-phase inverter control system. In order to simplify the analysis, this paper simplifies the VSG model:

(1) Adopt the three-phase hidden stage synchronous generator model to avoid uneven air gap.

(2) Assume that the polar logarithm P = 1.

(3) Ignore the factors such as core magnetic saturation and eddy current.

1) MECHANICAL MODEL

The rotor motion equation of the equivalent virtual synchronous machine is shown in (1):

$$\begin{cases} J\dfrac{d\omega}{dt} = T_{\mathrm{m}} - T_{\mathrm{e}} - T_{\mathrm{d}} = T_{\mathrm{m}} - T_{\mathrm{e}} - D\left(\omega - \omega_0\right) \\ \dfrac{d\theta}{dt} = \omega \\ \delta = \displaystyle\int \omega - \omega_0 dt \end{cases} \tag{1}$$

In the (1), the J is the moment of inertia of the synchronous generator,the unit is $kg \cdot m^2$; the T_m is the mechanical torque of the synchronous generator; the T_e is the electromagnetic torque, and the T_d is the damping torque considering mechanical wear, stator loss, damping winding, the unit is $N \cdot m$; the D is the damping coefficient corresponding to the damping torque, the unit is $N \cdot m{\cdot}s/rad$; ω, ω_0 are the mechanical angular velocity and the rated angular velocity, respectively, the unit is rad/s; θ is the angle between the axis of the A-phase stator and the axis of the rotating magnetic field. The electromagnetic torque of the generator can be obtained by the virtual electromotive force e_{abc} of VSG and the output current i_{abc} of VSG [11].

$$T_{\mathrm{e}} = \frac{P_e}{\omega} = \frac{e_a i_a + e_b i_b + e_c i_c}{\omega} \tag{2}$$

In the (2), the P_e is the electromagnetic power output of the VSG, the e_{abc} is the virtual electromotive force of the VSG, and the i_{abc} is the output current of the VSG.

2) ELECTROMAGNETIC MODEL

The electromagnetic equation of VSG can be obtained from Fig. 2:

$$L\frac{di_{abc}}{dt} = e_{abc} - u_{abc} - Ri_{abc} \tag{3}$$

In the (3), L and R are the synchronous reactance and resistance of the analog synchronous motor, and u_{abc} is the terminal voltage of the analog synchronous motor. In the actual controller, L and R can be inconsistent with the filter inductance and equivalent resistance in the inverter main circuit.

When the synchronous generator is running stably, it is assumed that the excitation current is a constant value and its rate of change is 0, the internal potentials e_a, e_b, and e_c are simplified to:

$$\begin{cases} e_a = E\sin\theta \\ e_b = E\sin\left(\theta - \dfrac{2\pi}{3}\right) \\ e_b = E\sin\left(\theta - \dfrac{4\pi}{3}\right) \end{cases} \tag{4}$$

In the (4), the E is the internal potential amplitude, and its expression can be written as:

$$E = \omega M_f i_f \tag{5}$$

In the (5), the ω is the angular frequency of the rotor; the M_f is the maximum mutual inductance between the stator and rotor windings; the i_f is the excitation current.

Combining the above formula, because of the J, the grid-connected inverter has inertia, thereby adjusting the frequency and power fluctuations of the power system. Due to the D, the inverter has a restraining effect on grid power oscillation. The traditional synchronous generator control system changes the active power of the system by controlling the mechanical torque T_m, by changing the system excitation current i_f, and then controls the amplitude of the internal potential e_{abc}. The VSG technology draws on this principle to realize the active-frequency and reactive-voltage regulation of the system.

B. THE VSG CONTROL STRATEGY

1) VIRTUAL GOVERNOR AND ACTIVE POWER FREQUENCY REGULATION

When the system load of the microgrid changes, the system should have a certain frequency support to ensure the stability of the microgrid. The synchronous generator set realizes the active power-frequency adjustment of the system through the prime mover governor. The prime mover governor equation is:

$$P_m = P_{ref} + k_f(\omega_0 - \omega) \tag{6}$$

In the (6), P_m is the active power output by the synchronous generator, P_{ref} is the active power given value, the unit is W, and k_f is the adjustment coefficient. From $P = T * \omega$, the relationship between the mechanical torque and the angular frequency of the output voltage can be obtained, combined with (1), the rotor motion equation after frequency modulation can be obtained:

$$J\frac{d\omega}{dt} = \frac{P_{ref}}{\omega_0} + \frac{k_f}{\omega_0}(\omega_0 - \omega) - T_e - D(\omega - \omega_0) \tag{7}$$

From (7), it can be seen that the damping coefficient of the system increases equivalently after frequency modulation [10].

Simultaneous (1), (6), (7)

$$\frac{\Delta\omega}{\Delta P} = \frac{\omega_0 - \omega}{P_{\text{ref}} - P_e} = -\frac{1}{J\omega_0 s + D\omega_0 + k_f} = -\frac{m}{\tau s + 1} \tag{8}$$

$$\begin{cases} \tau = \dfrac{J\omega_0}{D\omega_0 + k_f} \\ m = \dfrac{1}{D\omega_0 + k_f} \end{cases} \tag{9}$$

In the (9), τ is the inertial time constant, m is the active power droop coefficient [12].

It can be seen from the (8) and (9), the active frequency control using VSG adds an inertia link compared to the traditional active frequency control, which adjusts the frequency deviation of the access point and realizes the control of the J.

Combining the active power-frequency adjustment relationship of the synchronous generator and its rotor motion equation, the VSG virtual governor is designed to realize the active power-frequency regulation. As shown in Fig.3, it is the control block diagram of the VSG virtual governor and active power-frequency regulation.

2) VIRTUAL EXCITER AND REACTIVE POWER-VOLTAGE REGULATION

In addition to the above-mentioned frequency modulation function, the synchronous generator can also change the reactive power output to realize the voltage regulation function. The excitation controller is added to the synchronous generator control system to adjust the output voltage by adjusting the excitation current. Based on this principle, the closed loop

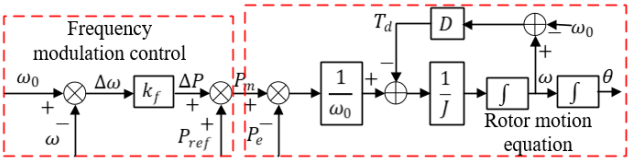

FIGURE 3. Control block diagram of virtual governor and active power-frequency adjustment.

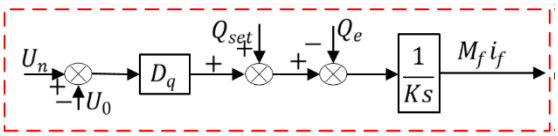

FIGURE 4. Reactive power-voltage regulation diagram.

equation of the VSG virtual exciter is [13]:

$$i_f = G(s)(U_{ref} - U) \tag{10}$$

In the (10), the U_{ref} is the reference voltage; the U is the VSG output voltage; the G(s) is the excitation regulator to ensure that the VSG output voltage follows the reference voltage, and G(s) is the integral regulator.

The equation of reference voltage change with reactive power is.

$$U_{\text{ref}} = U_n + \frac{1}{D_q}(Q_{set} - Q_e) \tag{11}$$

In the (11), the U_n is the rated output voltage; the D_q is the reactive power-voltage droop coefficient; the Q_{set} is the reactive power; the Q_e is the actual reactive power output by the VSG.

Combining (10) and (11), the closed-loop equation of the excitation controller can be obtained after considering the voltage regulation. The above detailed analysis can be found in [2], [24].

$$i_f = \frac{G(s)}{D_q}\left[U_n - U_0 + \frac{1}{D_q}(Q_{set} - Q_e)\right] \tag{12}$$

According to (12), the control block diagram of the reactive power loop of the synchronous generator with excitation control and reactive-voltage control can be obtained.

The control block diagram of the virtual synchronous generator is shown in Fig.5. The VSG control strategy mainly includes active power regulation and reactive power regulation. The active power regulation simulates the frequency modulation characteristics of the synchronous generator and the rotor motion equation. In reactive power regulation, virtual excitation regulation and reactive power regulation are established, which together determine the VSG rotation angle and phase voltage amplitude.

III. ANALYSIS OF VIRTUAL SYNCHRONOUS GENERATOR CONTROL SYSTEM

This paper combines the equivalent relationship between distributed power sources and synchronous generators, analyzes

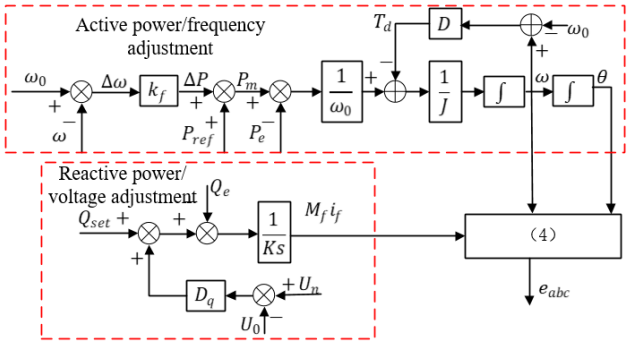

FIGURE 5. VSG control block diagram.

the impact of various parameter changes on the stability and dynamic performance of the power grid, and focuses on the impact of changes in J and D values on the system. Fig.6 is the equivalent circuit diagram of VSG grid-connected.

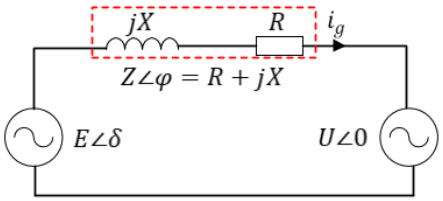

FIGURE 6. Equivalent circuit diagram when VSG is connected to the grid.

To simplify the analysis, and because $X \gg R$, ignoring the influence of resistance, when the VSG output impedance is purely inductive, the available VSG output active and reactive power are:

$$\begin{cases} P = \dfrac{EU}{X}\sin\delta \\ Q = \dfrac{EU\cos\delta - U^2}{X} \end{cases} \tag{13}$$

In the (13), E is the inner electric potential within the VSG; U is the voltage in PCC; X is the VSG output filter impedance; φ is the impedance angle, and δ is the VSG output power angle. Usually the δ is very small, $\sin\delta \approx \delta$, $\cos\delta \approx 1$,the (13) can be further simplified as:

$$\begin{cases} P = \dfrac{EU}{X}\delta \\ Q = \dfrac{EU - U^2}{X} \end{cases} \tag{14}$$

It can be seen from the above formula that the active power is closely related to the power angle, and the reactive power mainly depends on the voltage amplitude. In the (14), $K_t = \frac{EU}{X}$, K_t is the VSG torque coefficient [25]. Combined with (1) and (8), a linearized small model model can be obtained, and the negative feedback is simplified, and the simplified small signal model can be obtained as shown in Fig.7.

The specific adjustment process is: when the system is disturbed or the load changes, assume $P_{ref} > P_e$, the frequency

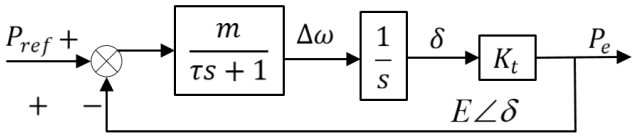

FIGURE 7. Small signal model of virtual synchronous generator.

deviation $\Delta\omega$ is obtained from the rotor motion equation, and the power angle increases $\Delta\delta$ after integration. At this time, the VSG output active power increases, and conversely, the active power decreases.

$$\begin{cases} G(\mathrm{s}) = \dfrac{\mathrm{mK_t}}{(\tau\mathrm{s}+1)\,\mathrm{s}} \\ \Phi\,(\mathrm{s}) = \dfrac{\frac{\mathrm{mK_t}}{\tau}}{s^2 + \frac{1}{\tau}s + \frac{\mathrm{mK_t}}{\tau}} \end{cases} \tag{15}$$

$G\,(s)$ is the open-loop transfer function, and $\Phi\,(s)$ is the closed-loop transfer function, which is a typical second-order transfer function. It can be seen from (9) that, $\tau = J\omega_0/(D\omega_0 + K_f), m = 1/D\omega_0 + K_f$. The virtual inertia and damping coefficient determine the dynamic response performance of the system. The natural oscillation angular frequency ω_n and the damping ratio ξ of the second-order model can be obtained:

$$\begin{cases} \omega_n = \sqrt{\dfrac{\mathrm{mK_t}}{\tau}} \\ \zeta = \dfrac{1}{2\sqrt{\mathrm{mK_t}\tau}} \end{cases} \tag{16}$$

The time response of the second-order system mainly depends on the two parameters ω_n and ξ. For the traditional synchronous generator system, ω_n and ξ remain unchanged. For VSG control, the choice of virtual moment of inertia and damping is more flexible. The natural oscillation frequency of the synchronous generator (0.628-15.700rad/s) can be used for reference, combined with (16) to determine the required virtual inertia range, and the optimal damping ratio of the second-order system is 0.707. The required range of the D can also be determined by (16).

In order to analyze the role played by the virtual inertia machine damping coefficient in the system adjustment process. Under the unit step response, different J and D are selected to observe the dynamic performance of the system. Fig.8 shows the unit step response of VSG under different moments of inertia and damping coefficient.

In the dynamic response process, the influence of different J and D on the system response performance in the time domain can be obtained. Table 1 shows the impact of parameter changes on the dynamic performance of the second-order system, including overshoot $\sigma\%$ and adjustment time t_s.

The moment of inertia determines the oscillation frequency during the dynamic response of the VSG active power. The damping coefficient D determines the decay rate during the dynamic response of the VSG active power [9].

Fig.9 is the Bode plot of the active power transfer function, by comparing the schemes 1, 2, and 3, it can be seen that

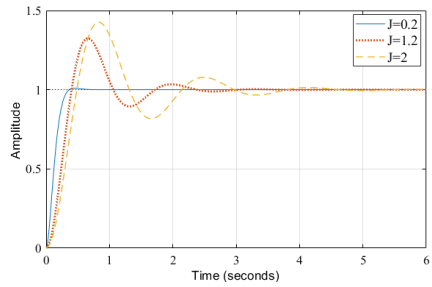

(a) $D = 5\ N \cdot m \cdot s/rad$

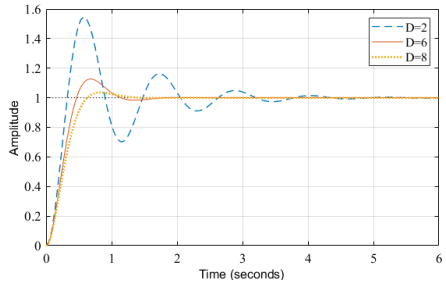

(b) $J = 0.5\ kg \cdot m^2$

FIGURE 8. VSG unit step response under different moments of inertia and damping coefficient.

TABLE 1. The influence of the J and the D on the time domain response performance.

J	D	ξ	$\sigma\%$	t_s
Increase	Constant	Decrease	Increase	Increase
Constant	Increase	Increase	Decrease	Decrease

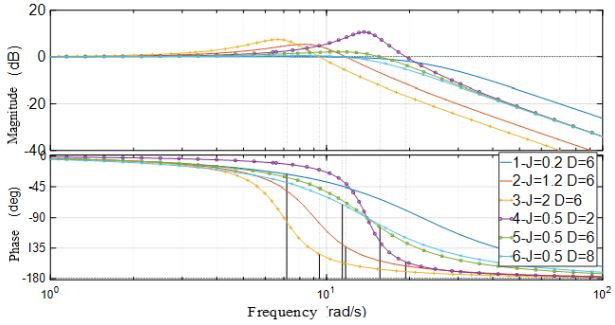

FIGURE 9. Bode plot.

different J determine the bandwidth and oscillation frequency of the dynamic response. Comparing schemes 3, 4, and 5, it can be seen that the damping coefficient has a better suppression effect on the resonance peak.

When ignoring the damping term, from (1), we can get:

$$\frac{d\omega}{dt} = \frac{P_{ref} - P}{J\omega_0} \tag{17}$$

When the active frequency difference is within a certain range, the angular frequency change is inversely proportional to the J, and the relationship between the system frequency change rate and the moment of inertia is deduced [26]:

$$\frac{df}{dt} \propto \frac{1}{J} \tag{18}$$

It can be seen from (18) that the larger the moment of inertia J is set, the smaller the system frequency fluctuation and the more stable the system, but judging from the unit step response of the system, the J cannot be set too large, otherwise the stability of the system will deteriorate.

When considering the damping term, it can be seen from (1) that when $T_m - T_e - J\frac{d\omega}{dt}$ remains constant, the greater the damping D, the smaller the frequency deviation $\Delta\omega$,Therefore, it is necessary to set the parameters reasonably to ensure the reliable operation of the system. Based on this, this paper expands the parameter setting and analysis based on the optimal damping ratio, and sets the parameters flexibly according to the system characteristics.

IV. ADAPTIVE CONTROL STRATEGY AND PARAMETER SETTING

A. THE VSG PARAMATER COOPERATIVE ADAPTIVE CONTROL STRATEGY

During the operation of the microgrid, new energy sources are the main output, which has strong volatility, causing changes in the input power, which in turn affects the stable operation of the microgrid. The oscillation process of the system was studied under the VSG control strategy, and the power Angle characteristics and angular frequency oscillation curves were analyzed from the power characteristics of the hidden pole synchronous generator, as shown in Fig. 10.

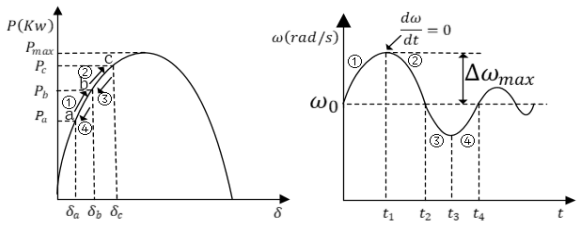

(a) Power angle characteristic curve.(b) Angular frequency oscillation curve

FIGURE 10. Schematic diagram of power angle curve and angular frequency oscillation process.

Combined with Fig.10, the variation of power and frequency in the switching process of working point during system operation is explained. When the system runs stably at point a, the corresponding VSG input active power is P_a, and the corresponding power angle is δ_a, When the system is disturbed, the active power of the system jumps to P_b, The oscillation process of the system is divided into 4 stages. In the process of $t_0 - t_1$, the VSG input active power increases, and its virtual rotor angular frequency $\omega > \omega_0$, At the same time, the rate of change of angular frequency $d\omega/dt$ increases first and then decreases gradually, but always stays $d\omega/dt > 0$, a larger J damping D is required. However, it can be seen from the analysis in Section 2, the larger J

makes the dynamic performance of the system worse, and the size of J needs to be selected reasonably; When the system is at operating point b, the input and output active power is balanced. Due to the inertia of the system, the operating point continues to change. In the $t_1 - t_2$ process, the rotor's angular velocity enters the deceleration process, maintaining $d\omega/dt < 0$, But the virtual rotor angular frequency $\omega > \omega\_0$, at this time,the system should reduce the J to make the system accelerate and return to a steady state. In the subsequent stage of $t_2 - t_3$, the operating point moves to b, and the rotor angular frequency is inconsistent with the system. Then move to point a and enter the $t_3 - t_4$ period. When the system resumes stable operation, the oscillation process ①-④ will be repeated continuously.

To sum up, the value of the moment of inertia is related to the amount of change and rate of change of the virtual rotor angular frequency. Under different working conditions, the selection principle of the rotor inertia is shown in Table 2.

According to the relationship between the moment of inertia and the change of the rotor angular frequency and the rate of change in Table 2. Combining the control strategy proposed in the [13], [24]–[26], an adaptive strategy based on the optimal damping ratio of the VSG moment of inertia and damping cooperative control is proposed. The moment of inertia control strategy is as follows:

$$J = \begin{cases} \textbf{i} \quad \boldsymbol{J_0 - k_i \Delta\omega} \\ \Delta\omega\,(d\omega/dt) \le 0 \cap |d\omega/dt| \le K \\ \textbf{ii} \quad \boldsymbol{J_0}\,|d\omega/dt| \le K \\ \textbf{iii} \quad \boldsymbol{J_0 + k_j \Delta\omega\,(d\omega/dt)} \\ \Delta\omega\,(d\omega/dt) > 0 \cap |d\omega/dt| > K \end{cases} \tag{19}$$

TABLE 2. Selection principle of moment of inertia J under different working conditions.

Condition	$\Delta\omega$	$d\omega/dt$	$\Delta\omega(d\omega/dt)$	J
①	>0	>0	>0	Increase
②	>0	<0	<0	Decrease
③	<0	<0	>0	Increase
④	<0	>0	<0	Decrease

In the (19), the J_0 is stable value of the moment of inertia when the power fluctuation is relatively small in the micro grid, the K is the limited value of the frequency deviation rate, and the k_j is the adjustment coefficient of the frequency variation.

The value of the damping coefficient D can be obtained by combining formulas (15) (19):

$$D = 2\xi\sqrt{\frac{JEU}{X\omega_0}} - \frac{k_f}{\omega_0} \tag{20}$$

Let $C_1 = 2\xi\sqrt{EU/X\omega_0}, C_2 = k_f/\omega_0$, then $D = C_1\sqrt{J} - C_2$. In this paper, the optimal damping ratio of the second-order system $\xi = \sqrt{2}/2$ is selected to obtain the relationship between the J and the D. The formula for D can be derived from formulas (19) (20), This article discusses J in detail, so the expression of D will not be analyzed in detail.

In order to have good response characteristics during the dynamic response process of the VSG, the control strategy discussed in the article adjusts the J, the D, f, and P to the appropriate control. When the system is disturbed, the J and the D can adjust their own value adaptively according to the changes of frequency and frequency change rate, so that the system can quickly restore stability. At the same time, it is necessary to analyze the rationality of the J, the D, and k_f.

B. VSG PARAMETER TUNING

In the VSG parameter coordinated adaptive control strategy, the J and damping D can be flexibly set according to the operating state of the microgrid. The selection of different parameters has a certain impact on the stable operation of the system, and it needs to be designed reasonably according to different situations.

From the above mentioned the natural oscillation frequency range of the synchronous generator (0.628-15.700rad/s), combined with the formula (9) (16), calculates the virtual moment of inertia range of the VSG:

$$4 \times 10^{-3}\frac{EU}{X\omega_0} \le J \le 2.5\frac{EU}{X\omega_0} \tag{21}$$

At the same time, the (15) can find the characteristic root of the second-order system as:

$$P_{1,2} = -\frac{D\omega_0 + k_f}{2J\omega_0} \pm \sqrt{\left(\frac{D\omega_0 + k_f}{2J\omega_0}\right)^2 - \frac{EU}{XJ\omega_0}} \tag{22}$$

Since $D\omega_0 + k_f$ is a positive value, in order to ensure the stability of the system, the J needs to be kept greater than zero when it changes. The minimum value of the J is known from (19):

$$J_{min} = J_0 - k_j\Delta\omega_{max} \tag{23}$$

Similarly, the value of the D can be derived from the J. According to the adaptive control strategy, the values of J and D are mainly changed by the limit value K, When $d\omega/dt$ is small, reduce the J and the D; when it exceeds K, increase J and D appropriately. Combining (1), the value range of K is:

$$0 \le K \le \left|\frac{1}{J}\left(\frac{\Delta P}{\omega_0} - D\Delta\omega\right)\right| \tag{24}$$

The value of K is related to the J, the D, the angular frequency deviation $\Delta\omega$ during system operation, and the frequency deviation ΔP, Therefore, the value of K should be reasonably planned to ensure the stable operation of the system.

For the value of the adjustment coefficients k_j and k_i, the deviation between the rated power of the microgrid and the maximum angular frequency of the system should be

considered [20]. Take k_j as an example to calculate the value of the adjustment coefficient:

$$k_j = \frac{J_{\max} - J_0}{\Delta\omega\,(d\omega/dt)} \tag{25}$$

In the (25), when the damping term is ignored, $J_{max} = \Delta P/(\Delta\omega * \omega_0)$, According to iii in (19), set J_0 to 0.5, and draw a three-dimensional graph of the J changing with the adjustment coefficient k_j, as shown in Fig.11:

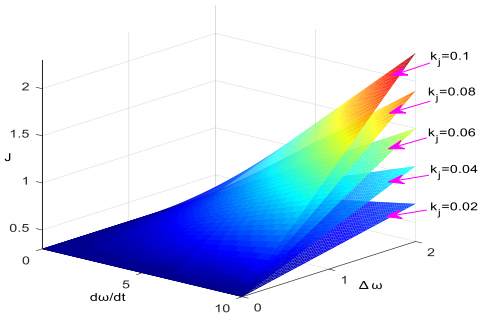

FIGURE 11. Moment of inertia change value under different k_j.

It can be seen from Fig.11 that with the increase of the adjustment coefficient k_j, the increase of the J gradually becomes faster, and the sensitivity of the angular frequency transformation amount and the rate of change also increases. When the system is disturbed, the J will increase rapidly, so the adjustment coefficient k_j needs to be reasonably selected according to the system capacity.

According to the (22), draw the root locus for different J and D. Fig.12 shows the root locus for parameter changes.

When the D is constant, with the increase of J, the closed-loop pole of the system approaches the imaginary axis, its effect on the system becomes more obvious, and the dynamic performance of the system becomes worse. Therefore, the value of the J should not be too large; When the J is constant, with the increase of the D, the imaginary part of the closed-loop poles gradually becomes smaller, and they meet and separate at the real axis, indicating that the system changes from under-damped to over-damped. If the D is too small, the adjustment coefficient k_f plays a major role. At this time, the damping effect of the system is poor and the system is easy to lose stability. From the previous analysis, it can be known that the adjustment coefficient k_j, the angular frequency change limit value K and other parameters have a certain impact on the values of the J and the D, and then affect the stable operation of the microgrid.

V. SIMULATION ANALYSIS

In order to verify the effectiveness of the proposed control strategy and the influence of the J and the D on the stability of the microgrid during operation, the VSG model was built in MATLAB/Simlink for simulation experiment verification. The simulation parameters are shown in Table 3.

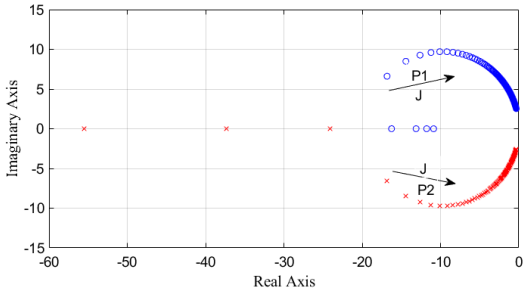

（a）$D = 5\ N\cdot m\cdot s/rad, J: 0.1\sim15\ kg\cdot m^2$

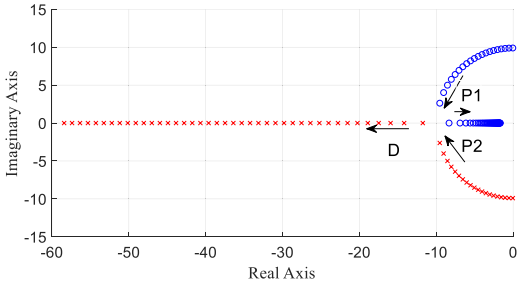

(b) $J = 0.8\ kg\cdot m^2, D: 0\sim40N\cdot m\cdot s/rad$

FIGURE 12. Root locus under parameter changes.

TABLE 3. Simulat ameters.

Symbol	Value	Symbol	Value
U_{dc}/V	700	J_0	0.3
U_n/V	220	D_0	5
L_f、L_g/mH	3、3	k_f	20
$C/\mu F$	25	K	2.5
R_f、R_g/Ω	0.1、0.6	k_j	0.03
ω_0/(rad/s)	314	k_i	1.5

A. THE VSG ACTIVE POWER STEP SIMULATION EXPERIMENT

From the previous analysis, we can see that the J and D have a greater impact on the active power and frequency of the system. In order to verify the influence of different parameters on the stability of the system, the VSG simulation model was built with a system simulation step of 1.5 seconds. The given value of VSG active power is 5kW, and the reactive power is 6kvar. At 0.4s, the system active power becomes 15kW. Under this system condition, observe the influence of different parameters on the system. Fig.13 shows the effect of the VSG moment of inertia on the system, keeping the D constant, Fig.13(a) is the change of the system's active power output under different J, Fig.13(b) is the change of the system's angular frequency under different J.

It can be seen from Fig.13(a) that when the J takes the values 0.2, 0.4, 0.6, 0.8 $kg\cdot m^2$, the system output active power overshoot is 36.7%, 34.5%, 29.3%, 27%, and the adjustment time is 0.9s, 0.83s, 0.71s, 0.59s, As the J increases, the

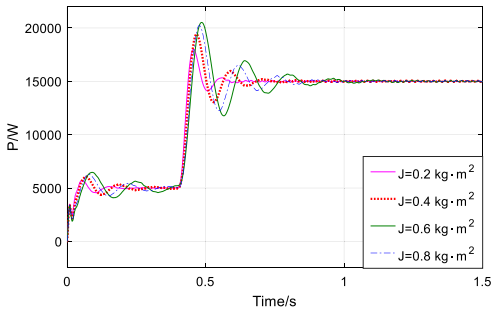

(a) System active power output under different moments of the J

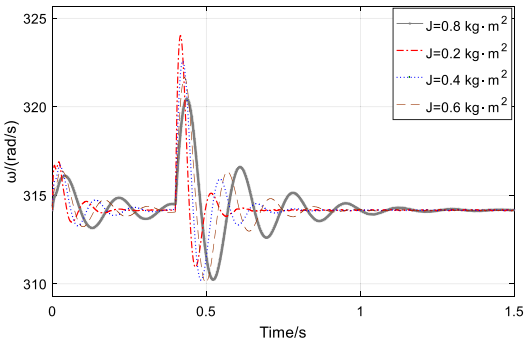

(b) The angular frequency of system rotation changes under different *J*.

FIGURE 13. The influence of VSG moment of inertia on the system.

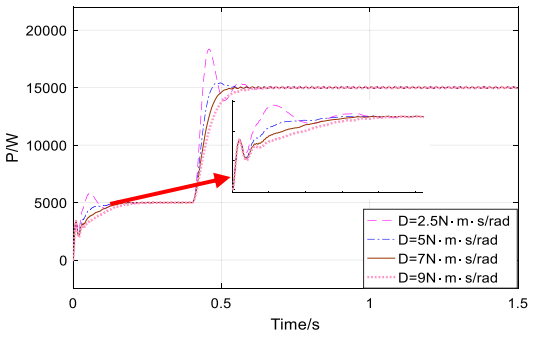

(a) System active power output under different D.

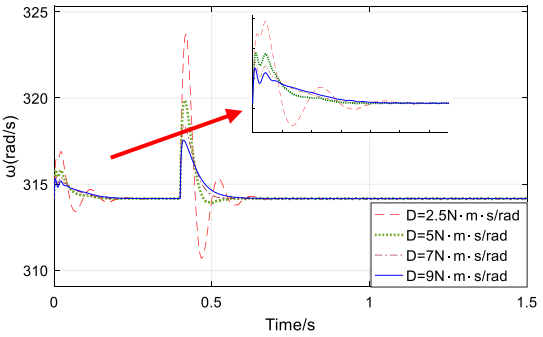

(b) The system rotation angular frequency changes under different D

FIGURE 14. VSG damping affects the system.

suppression of the active power fluctuation of the system weakens, which is consistent with the root locus analysis results; It can be seen from Fig.13(b) that the overshoot of the system output angular frequency ω is 3.2%, 2.7%, 2.3%, 2.1%, the adjustment time is 0.62s, 0.72s, 0.83s, 0.103s, and the increase of the J will suppress the fluctuation of the system frequency, but at the same time will weaken the system damping.

When the value of the J calculated from the optimal damping ratio is 0.2∼0.8, the corresponding damping is 4.4∼8.9. In order to compare the impact of damping on the system, keeping the J unchanged, take the D to be 2.5, 5, 7, 9 $N \cdot m \cdot s/rad$ to observe the changes in the system output active power and angular frequency. Fig.14 shows the effect of VSG damping on the system, (a) is the system active power output under different D, (b) is the system rotation angular frequency change under different D.

It can be seen from Fig.14 that when the active power step occurs in the system, the increase of damping can suppress the overshoot of the active power and angular frequency of the system, which is consistent with the conclusion of the root locus analysis above. However, as the D increases, the adjustment time gradually increases. When the system is initially given active power, the phenomenon is more obvious, that is, the lower the system active power, the stronger the effect of the same damping on the system.

B. MULTIPART FIGURES SIMULATION EXPERIMENT UNDER DIFFERENT CONTROL MODES

In order to verify the effectiveness and superiority of the control strategy of this article, it is compared with the existing control method under the system grid connection mode. Scheme 1 is the constant parameter control, the J is $0.35kg \cdot m^2$ and the D is selected to be 7.5 $N \cdot m \cdot s/rad$; Scheme 2 is variable parameter control [15], [16] bang-bang control strategy, $J_{min} = 0.35kg \cdot m^2$,$J_{max} = 1kg \cdot m^2$; Scheme 3 is the control strategy proposed in this paper, take $J_0 = 0.35kg \cdot m^2$.

In this case, the system simulation step length is 1.5 seconds, the given value of VSG active power is 5kW, and the reactive power is 6kvar. At 0.5 second, the system active power becomes 10kW, and at 1 second, the system active power drops to 5kW. Observe and compare the effectiveness of different strategies under system conditions.

Fig.15 is a comparison diagram of system active power changes under three different control strategies. It can be

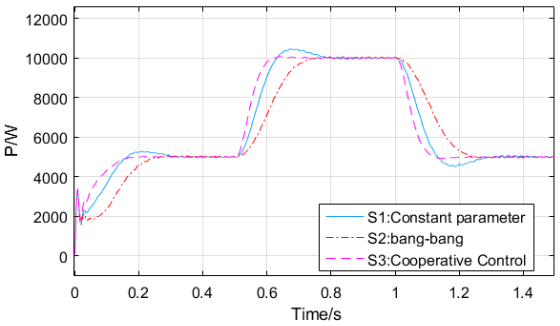

FIGURE 15. Comparison of system active power changes under three control strategies.

seen from the figure that the proposed control strategy shows better dynamic change characteristics in the active power fluctuation range and tracking performance than the other two control methods. The performance is that when the system active power suddenly increases to 10kW at 0.5s, there is overshoot under the constant parameter control strategy in the first scheme, the system adjustment time of the second scheme is too long, and the third scheme is based on the VSG coordination of the optimal damping ratio, it speeds up the response time of the system and suppresses frequency overshoot, the power changes smoothly, and the transient performance is better.

When the system active power changes in Fig.15, the system characteristics are summarized as Table 4. Table 4 is the comparison of system features under three different control strategies. The specific comparison time is 0.5s and 1s when the system active power increases and decreases. The comparison parameter is the system overshoot $\sigma\%$ and adjustment time t_s. When the system active power changes, among the three schemes, the system active power under the control strategy proposed in this paper has no overshoot and the adjustment time is the shortest.

TABLE 4. Comparison of system active dynamic performance parameters under three different control strategies.

Time	0.5s			1s		
scheme	S1	S2	S3	S1	S2	S3
$\sigma\%$	5	0	0	5	0	0
t_s	0.29	0.24	0.12	0.28	0.22	0.12

Fig.16 shows the comparison of effects under different control strategies, the Fig.16(a) is the comparison of system frequency changes under different schemes, and the Fig.16(b) is the current waveform under scheme 1 and scheme 3.

Comparing schemes 1 and 2, when the D is the same, the J in the bang-bang control will choose its own size when the system is disturbed. Although the change of J is discontinuous, compared with the fixed parameter, the bang-bang control strategy suppresses the frequency fluctuation to a certain extent. Comparing schemes 2 and 3, because scheme 3 changes the J and D coordinately when the system is disturbed, it has a better effect on coping with sudden increase or decrease of system active power. From the comparison of the current waveforms in Fig.16(b), the current fluctuations are more obvious under certain parameters, while the current changes smoothly under cooperative control. In summary, the VSG cooperative control strategy based on the optimal damping ratio proposed in this paper can better cope with the instability caused by the microgrid, especially the new energy power generation, and further improve the robustness of the system.

Fig.17 is the change of the J under the two control strategies. Fig.17(a) is the change of the J under the bang-bang control strategy, and Fig.17(b) is the change of the J under the cooperative control strategy proposed in this paper. When

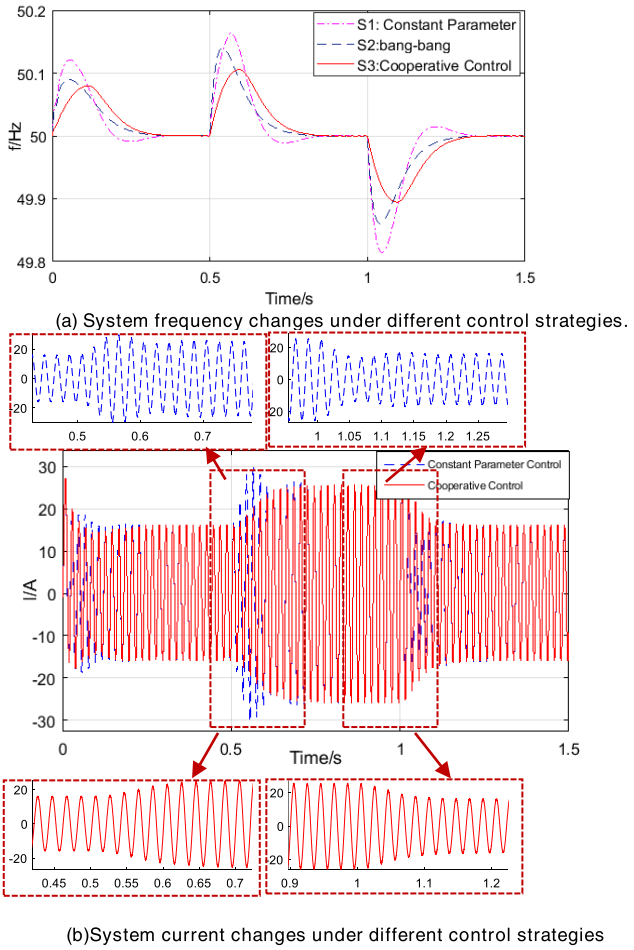

(a) System frequency changes under different control strategies.

(b)System current changes under different control strategies

FIGURE 16. Effect comparison.

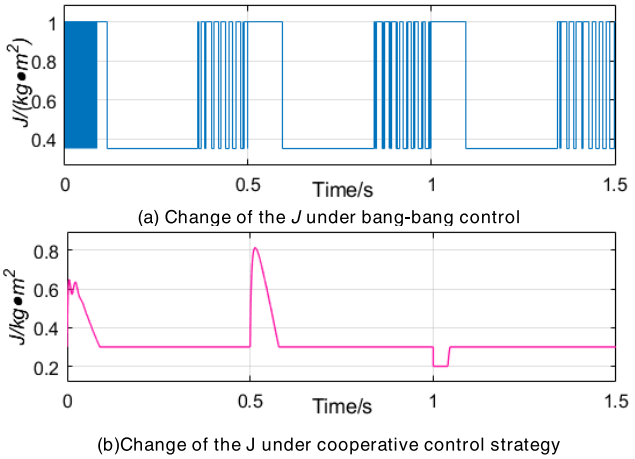

(a) Change of the J under bang-bang control

(b)Change of the J under cooperative control strategy

FIGURE 17. Change of the J under two different control strategies.

the power suddenly increases or decreases, it can be seen from the Fig.17(a) that under the bang-bang control strategy, the J changes between the J_{max} and the J_{min} to suppress the system oscillation, but the excessive J increases the system adjustment time, and the frequent switching of the J will

cause certain harm to the stability of the system; Fig.17(b) shows that at the moment when the active power of the system changes suddenly, under the coordinated control strategy in this paper, the J responds quickly and drops rapidly to form a spike, which suppresses the system oscillation while reducing the adjustment time, it avoid frequent switching of the J affecting the stability of the system.

VI. CONCLUSION

Regarding the uncertainty and poor anti-interference ability of distributed new energy generation, based on the VSG control strategy, this paper proposes the VSG collaborative control strategy based on the optimal damping ratio, and the conclusions are as follows:

1) The algorithm links the VSG moment of inertia and damping through the optimal damping ratio. Based on the frequency change rate and the amount of change, combined with the synchronous generator power angle curve, the control strategy expression is obtained to realize the coordinated control of the parameters.

2) The influence of the moment of inertia and damping change on the dynamic performance of the system is analyzed in detail, which makes a useful exploration for the research of the VSG control technology.

3) The effectiveness of the proposed control strategy is verified through simulation, and the dynamic performance and anti-interference ability of the system are further improved through experimental comparison.

REFERENCES

[1] C. Liu, J. Zhuo, and D. Zhao, "A review on the utilization of energy storage system for the flexible and safe operation of renewable energy microgrids," *Proc. CSEE*, vol. 40, no. 1, pp. 1–18, 2020.

[2] L. Zhipeng, S. Wanxing, and L. Haitao, "Application and challenge of virtual synchronous machine technology in power system," *Proc. CSEE*, vol. 37, no. 2, pp. 349–359, 2017.

[3] J. Su, *Grid-connected Technology of Distributed Power and Microgrid*. Beijing, China: Electric Power Press of China, 2015, pp. 15–64.

[4] M. Ashabani and Y. A.-R.-I. Mohamed, "Novel comprehensive control framework for incorporating VSCs to smart power grids using bidirectional synchronous-VSC," *IEEE Trans. Power Syst.*, vol. 29, no. 2, pp. 943–957, Mar. 2014.

[5] L. Xiong, F. Zhuo, F. Wang, X. Liu, Y. Chen, M. Zhu, and H. Yi, "Static synchronous generator model: A new perspective to investigate dynamic characteristics and stability issues of grid-tied PWM inverter," *IEEE Trans. Power Electron.*, vol. 31, no. 9, pp. 6264–6280, Sep. 2016.

[6] S. D'Arco and J. A. Suul, "Equivalence of virtual synchronous machines and frequency-droops for converter-based MicroGrids," *IEEE Trans. Smart Grid*, vol. 5, no. 1, pp. 394–395, Jan. 2014.

[7] K. Sakimoto, Y. Miura, and T. Ise, "Stabilization of a power system including inverter-type distributed generators by a virtual synchronous generator," *Electr. Eng. Jpn.*, vol. 187, no. 3, pp. 7–17, May 2014.

[8] Q. C. Zhong and G. W. Synchronverters, "Synchronverters: Inverters that mimic synchronous generators," *IEEE Trans. Ind. Electron.*, vol. 58, no. 4, pp. 1259–1267, Apr. 2011.

[9] L. Zhipeng, S. Wanxing, and Z. Qingchang, "Virtual synchronous generator and its applications in micro-grid," *Proc. CSEE*, vol. 34, no. 16, pp. 2591–2603, 2014.

[10] H. Zhenxiang, *Analysis of Electric Power System*, 4th ed. Hangzhou, China: Zhejiang University Press, 2011, pp. 34–56.

[11] Y. Du, J. Su, M. Mao, and X. Yang, "Autonomous controller based on synchronous generator dq0 model for micro grid inverters," in *Proc. 8th Int. Conf. Power Electron.*, May 2011, pp. 2645–2649.

[12] L. Qu, *Power System Stability and Generator Excitation Control*. Beijing, China: Electric Power Press of China, 2015, pp. 34–79.

[13] S. Qiong, Z. Hui, S. Kai, and W. Yalong, "Improved adaptive control of inertia for virtual synchronous generators in islanding micro-grid with multiple distributed generation units," *Proc. CSEE*, vol. 37, no. 2, pp. 412–423, 2017.

[14] Z. Zuobing, H. Shaoping, and L. Zhenxing, "Research on control strategy of micro-grid adaptive damping VSG," *Control Eng. China*, vol. 1, no. 5, pp. 33–39, 2020.

[15] J. Alipoor, Y. Miura, and T. Ise, "Power system stabilization using virtual synchronous generator with alternating moment of inertia," *IEEE J. Emerg. Sel. Topics Power Electron.*, vol. 3, no. 2, pp. 451–458, Jun. 2015.

[16] F. Wang, L. Zhang, X. Feng, and H. Guo, "An adaptive control strategy for virtual synchronous generator," *IEEE Trans. Ind. Appl.*, vol. 54, no. 5, pp. 5124–5133, Sep./Oct. 2018.

[17] F. Wang, L. Zhang, X. Feng, and H. Guo, "Flexible virtual synchronous generator control for distributed generator with adaptive Inertiam," *Electr. Power Compon. Syst.*, vol. 47, pp. 128–140, Jan. 2019.

[18] S. M. Ashabani and Y. A.-R.-I. Mohamed, "A flexible control strategy for grid-connected and islanded microgrids with enhanced stability using nonlinear microgrid stabilizer," *IEEE Trans. Smart Grid*, vol. 3, no. 3, pp. 1291–1301, Sep. 2012.

[19] R. Rajan and F. M. Fernandez, "Power control strategy of photovoltaic plants for frequency regulation in a hybrid power system," *Int. J. Electr. Power Energy Syst.*, vol. 110, pp. 171–183, Sep. 2019.

[20] X. Quan, X. Zhao, L. Zhang, R. Xu, Y. Lei, and A. Q. Huang, "Novel power control of voltage-controlled inverters for grid inertia support," in *Proc. IEEE Appl. Power Electron. Conf. Expo. (APEC)*, Mar. 2019, pp. 927–931.

[21] Y. Yang, F. Mei, and C. Zhang, "Coordinated adaptive control strategy of rotational inertia and damping coefficient for virtual synchronous generator," *Electr. Power Automat. Equip.*, vol. 39 no. 3, pp. 125–131, 2019.

[22] M. H. Othman, H. Mokhlis, M. Mubin, S. Talpur, N. F. Ab Aziz, M. Dradi, and H. Mohamad, "Progress in control and coordination of energy storage system-based VSG: A review," *IET Renew. Power Gener.*, vol. 14, no. 2s, pp. 177–187, Feb. 2020.

[23] K. M. Cheema, "A comprehensive review of virtual synchronous generator," *Int. J. Electr. Power Energy Syst.*, vol. 120, Sep. 2020, Art. no. 106006.

[24] L. Xiankui, "A thesis submitted in partial fulllment of the requirements for the degree of master of engineering," M.S. thesis, Dept. Electron. Eng., Huazhong Univ.,Wuhan, China, 2015.

[25] J. Long, "Research on control strategy between island mode and grid-connected mode of micro-grid inverter based on virtual synchronous generator, " M.S. thesis, Dept. Electron. Eng., Jian Su Univ., Zheng Jian, China, 2018.

[26] C. Wen, D. Chen, and C. Hu, "Self-adaptive control of rotational inertia and damping coefficient of VSG for converters in a microgrid," *Automat. Electr. Power Syst.*, vol. 42, no. 17, pp. 120–126, 2018.

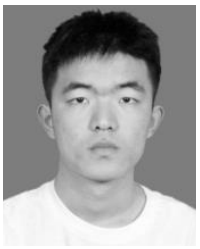

SHENGWEI QU received the B.E. degree in the electrical engineering and automation from the Jiangsu University of Science and Technology, China, in 2019. He is currently pursuing the M.Sc. degree with Shanghai Dianji University, Shanghai, China. His research interests include new energy power generation and microgrid technology.

ZHIJIE WANG received the Ph.D. degree from the China University of Mining and Technology, Xuzhou, China, in 2005. He is currently a Professor with the School of Electrical Engineering, Shanghai Dianji University. His research interests include new energy grid connection technology, variable frequency drive control technology, and fault diagnosis of large equipment.